MODELING OF THE INTERACTION BETWEEN A TURBULENT FLOW AND AN ABLATABLE MATERIAL

N. T-H. Nguyen-Bui *, T. Harribey *, P. Chassaing **
***C.E.A./CESTA, 33114, Le Barp, France,**
**** ISAE, 31056 Toulouse, France**
ngoc-thanh-ha.nguyen-bui@cea.fr

Keywords: *Ablation, turbulence, DNS, spectral forcing*

Abstract

During atmosphere reentry the probe heat shield suffers from a significant overheating. Composite materials undergo an ablative process that consumes the heat flux by physico-chemical reactions. Plasma jet experiments on polycrystalline graphite show a structural surface roughness like a scalloped pattern when the flow is turbulent. The goal of this study is to understand the interaction between a turbulent flow and an ablatable material at the smallest turbulent scale (the Kolmogorov scale). To this extent, direct numerical simulation (DNS) software has been developed and investigated. Firstly, in order to guarantee simulated patterns, the computed turbulence has been validated according to well-known results for turbulence decay and near-wall turbulence. Secondly, ablation experimentations have been performed to identify parameters responsible for turbulent roughness appearance.

1 Introduction

Ablative surface flows often arise when using thermal protection materials for preserving structural components of atmospheric re-entry spacecrafts.
During the atmospheric re-entry the heatshield of the probe suffers a significant overheating.
The composites materials undergo an ablative process that consumes the heat flux by physicochemical reactions. The composite disappears gradually by sublimation, oxidation. In the case of polycristalline graphite, plasma jet experiments show a structural surface roughness like a scalloped pattern when the flow is turbulent.
The main idea of this study is to characterize the interaction between a turbulent flow and an ablatable material at the Kolmogorov scale (the smallest turbulent scale).
The description of surface ablation is consequently very complex to model and requires knowledges and expertise in several disciplines such as chemistry and multicomponent physics, multi-phase ow dynamics, thermo-structural mechanics of composite materials, physics of particle/droplet impingement, roughness interaction mechanisms, or physics of radiative heat transfer.

Hence, the main objective of this work is to simulate this roughness and to understand the mechanisms that are responsible for it. Roughness lengthscale is about 50 µm which implies that the software implemented have to be able to consider very small lengthscales. This is why a DNS software has been chosen to compute flow evolution from the smallest lengthscale (Kolmogorov scale) to the largest (turbulent scale).

2 Modeling

2.1 Governing equations

Direct numerical simulation (DNS) is used to investigate the turbulence evolution. The flow is described by Navier-Stokes conservative balance equations for mass fraction for *ne* chemical species (1), momentum (2), and total energy (3):

$$\frac{\partial \rho C_\alpha}{\partial t} + \frac{\partial \rho u_j C_\alpha}{\partial x_j} = \frac{1}{\mathrm{ReSc}} \frac{\partial}{\partial x_j}\left(\rho D_\alpha \frac{\partial C_\alpha}{\partial x_j}\right) + \dot{\omega}_\alpha \quad (1)$$

$$\frac{\partial \rho u_i}{\partial t} + \frac{\partial \rho u_j u_i}{\partial x_j} = -\frac{1}{Ma^2}\frac{\partial p u_i}{\partial x_i} + F_i + \frac{1}{\mathrm{Re}}\frac{\partial}{\partial x_j}\left[\mu\left(\frac{\partial u_i}{\partial x_j} + \frac{\partial u_j}{\partial x_i} - \frac{2}{3}\frac{\partial u_l}{\partial x_l}\delta_{ij}\right)\right] \quad (2)$$

$$\frac{\partial \rho E}{\partial t} + \frac{\partial \rho u_j E}{\partial x_j} = -\frac{\partial p u_i}{\partial x_i} + \frac{Ma^2}{\mathrm{Re}}\frac{\partial}{\partial x_j}\left(\tau_{ij} u_i\right) + \frac{1}{\mathrm{RePr}}\frac{\partial}{\partial x_i}\left(\lambda \frac{\partial T}{\partial x_i}\right) + \frac{1}{\mathrm{ReSc}}\frac{\partial}{\partial x_i}\left(\sum_1^{n_e} \rho D_\alpha h_\alpha \frac{\partial C_\alpha}{\partial x_i}\right) + F_j u_j \quad (3)$$

where Re, Sc, Ma and Pr denote respectively the Reynolds number, the Schmidt number, the Mach number and the Prandtl number. Viscosity μ is defined by Sutherland's relation whereas thermal conductivity is $\lambda = \frac{\mu Cp}{\mathrm{Pr}}$.

2.2 Discretization

A 6th order compact finite difference scheme resolution describes the spatial discretization [1].

The grid resolution is a function of the Reynolds number and is in close agreement with other well-resolved simulations and Reynolds' predictions [2]. The smallest resolved scale is the Kolmogorov lengthscale η, its good resolution is ensured by the condition $\Delta x \le \frac{\eta}{2}$.

In the same extent, the computational box size of simulations is large enough so that the flow variables are not correlated across the computational box (Fig. 1). So, the box size is equal to about four times the wavelength of the peak energy.

A general method, derived from Poinsot & Lele [3], is used to specify boundary conditions for Navier-Stokes flows. This technique, called NSCBC is based on characteristic theory and includes a special treatment for viscous terms.

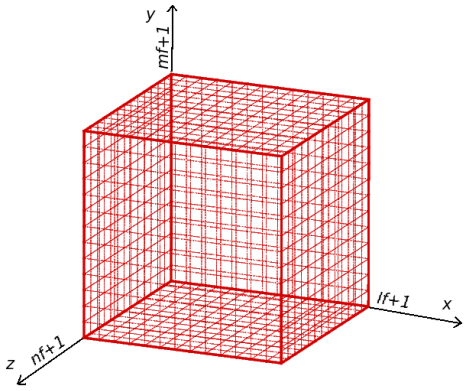

Fig. 1 Computational domain

Besides, an accurate coordinate transformation is implemented in order to take into account a roughness wall. This transformation is primordial to both describe the material recession and to maintain numerical scheme accuracy (which requires a constant spatial step).The 6th order of accuracy scheme is maintained by calculating the conform transformation [4].

Finally, a fourth order Runge-Kutta scheme is used for time discretization. The global time step is equal to the minimum between conductive and diffusive time steps and ensures the stability of explicit time discretization.

2.3 Initialization

To generate useful statistical quantities, an ensemble of ten independent flows was calculated and the results ensemble averaged. The homogeneous isotropic velocity field is initialized in spectral space using the Passot-Pouquet spectrum or the Von-Karman-Pao [5] spectrum. It is established by requiring that the initial velocity spectrum have a prescribed form and that the Fourier-transformed velocity field be random Gaussian variables. The approach is similar to that of Rogallo [6]. It consists in expressing the spectral velocity field norm as a function of energy spectrum:

$$\left\|\tilde{u}(\kappa_1,\kappa_2,\kappa_3)\right\|^2 = \frac{E(\kappa)}{2\pi\kappa^2}\Delta V_\kappa \quad (4)$$

where $\kappa = \sqrt{\kappa_1^2 + \kappa_2^2 + \kappa_3^2}$, and $(\kappa_1,\kappa_2,\kappa_3)$ is the coordinate system of a point in the spectral space. The Passot-Pouquet spectrum expression

implemented is

$$E(\kappa) = \frac{16u'^2}{\kappa_e}\sqrt{\frac{2}{\pi}}\left(\frac{\kappa}{\kappa_e}\right)^4 \exp\left[-2\left(\frac{\kappa}{\kappa_e}\right)^2\right] \quad (5)$$

where the averaged velocity u' is equal to $\sqrt{2k/3}$.

We have displayed on Fig. 2 two velocity fields extracted from Passot-Pouquet spectra with κ_e=4 (Fig. 2.a) and κ_e=10 (Fig. 2.b) using Fourier-transformation. κ_e is the wavenumber corresponding to the initial turbulent scale l_t with $\kappa_e = 2\pi/l_t$.

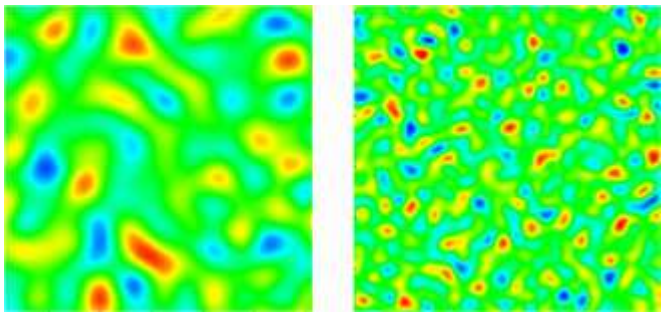

(a) κ_e=4 *(b)* κ_e=10

Fig. 2 Velocity fields obtained using Passot-Pouquet spectrum

FFTW library has been used to provide a faster the transition between spectral and physical space. This library turns out to be very convenient to implement a spectral forcing witch requires many transports between these two spaces.

3 Numerical Results

3.1 Simulation of an isotropic homogeneous turbulence (IHT)

The purpose of this part is to validate results obtained by computing isotropic turbulence decay. The theory developed for k-ε models is used to be compared to our DNS results. We consider an infinite space (periodic boundary conditions) where statistic properties remain constant by translation or rotation. There is neither mean flow nor diffusion. Considering those conditions, k-ε equation system becomes:

$$\frac{\partial k}{\partial t} = -\varepsilon$$
$$\frac{\partial \varepsilon}{\partial t} = -C_{\varepsilon,2}\frac{\varepsilon^2}{k} \quad (6)$$

The following expression of the couple (k-ε) is the exact solution of the system below:

$$k = k_0\left[1+(C_{\varepsilon,2}-1)\frac{t}{\tau_{k,t=0}}\right]^{\frac{1}{1-C_{\varepsilon,2}}}$$
$$\varepsilon = \varepsilon_0\left[1+(C_{\varepsilon,2}-1)\frac{t}{\tau_{k,t=0}}\right]^{\frac{C_{\varepsilon,2}}{1-C_{\varepsilon,2}}} \quad (7)$$

According to Comte-Bellot and Corrsin [7], the goal of this study is to evaluate the best power-law fit to inverse turbulent energy during the decay. In the case of an IHT, this power-law depends only on the value of $C_{\varepsilon,2}$. Fig. 3 shows that behaviors of the averaged kinetic energy k and the averaged dissipation rate fit perfectly with analytical solutions.

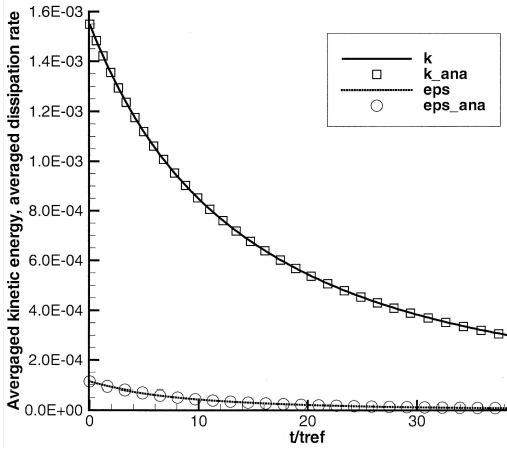

Fig. 3 Time evolution of k and ε compared to their analytical solutions (t_{ref} = 3,8.10^{-6} s)

$C_{\varepsilon,2}$ used in the analytical scheme turns out to be a function of the computed Reynolds number; its values are between 1.60 and 1.71 (greater Reynolds implies greater $C_{\varepsilon,2}$). These values are in close agreement with [7] for DNS experiments. To improve the physic representativeness of the computed turbulence, we have displayed evolution of isotropy components ratios (Fig. 4.a) and skewness and flatness factors of the velocity derivatives (Fig. 4.b) to both validate isotropy and homogeneity in the flow.

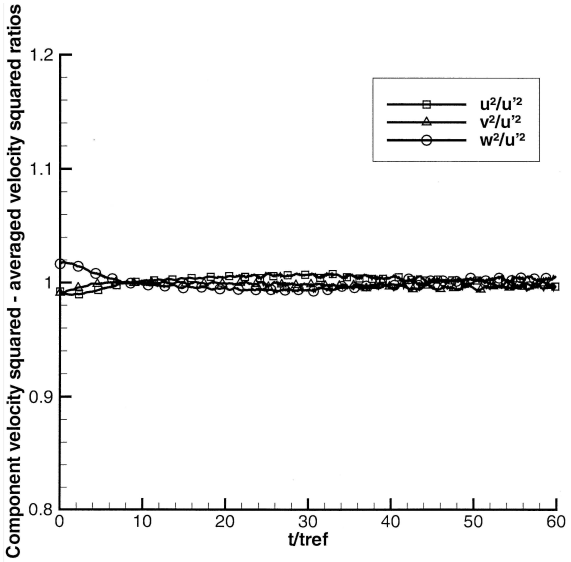

(a) Isotropy

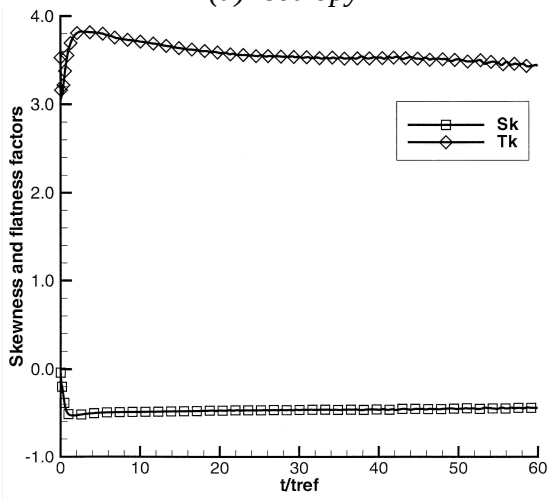

(b) Homogeneity

Fig. 4 Validation of IHT

The velocity-derivative skewness factor S_k and the flatness factor T_k are indicator of the self-preserving decay; their expressions are:

$$S_k = \frac{1}{3}\sum \frac{\overline{(\partial u_i / \partial x_i)^3}}{\overline{\left[(\partial u_i / \partial x_i)^2\right]^{3/2}}} \quad (8)$$

$$T_k = \frac{1}{3}\sum \frac{\overline{(\partial u_i / \partial x_i)^4}}{\overline{\left[(\partial u_i / \partial x_i)^2\right]^2}} \quad (9)$$

Expected values of approximately -0.5 for S_k and 3.5 for T_k have been reached until one large-eddy turnover time τ_k. These values are consistent with a good simulation of the IHT behavior.

3.2 Spectral forcing of turbulence

In DNS problem of turbulence, the field cannot be stationary if there is not external forcing, as turbulence is a dissipative system. So, a spectral forcing is used to generate a statistically steady turbulent flow.

The spectral forcing starts after a large-eddy turnover time τ_k witch is the time for the IHT to be established. The method consists of creating, in the spectral space, a new velocity field (kinetic energy and large-eddy wavenumber κ_e are user-defined). This field is added to the Fourier-transform of the current physical velocity field. Spectral forcing is performed as soon as averaged kinetic turbulent energy is lower more than one percent of its initial value $k(\tau_k)$.

Fig. 5 shows that the turbulent kinetic energy rate remains constant all along time simulation (Fig. 5.a). This artificially generated turbulence remains physically consistent, as proved by well known values of the skewness and flatness factors of the velocity derivatives (Fig. 5.b). Finally, we observe that different main lengthscales remain constant after $t = 2\tau_k$, preventing flow from degeneration (Fig. 5c).

The main advantage of this strategy is the possibility to choose properties of the flow like kinetic energy or the wavelength of large eddies κ_e. Consequently, we are able to force the flow using small structures (κ_e=20 for example), whereas it was initialized with a smaller wavenumber (κ_e=6). This method allows us to study the redistribution of kinetic energy by looking at the evolution of the spectrum $E(\kappa)$. It means that we can simulate the influence of turbulent roughness (witch generate small eddies) on a flow with large eddies.

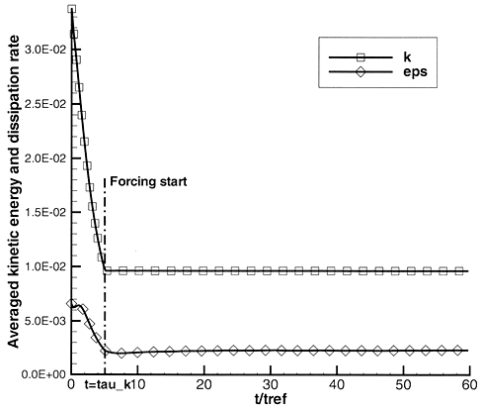

(a)

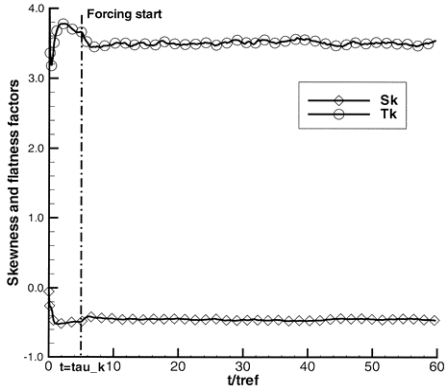

(b)

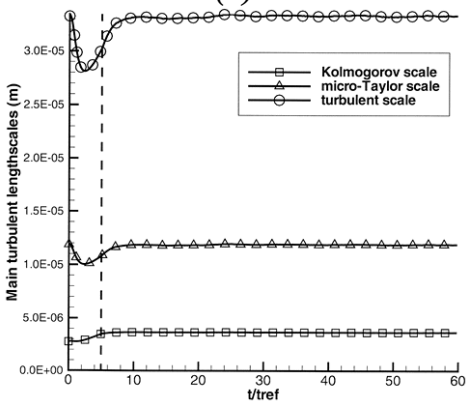

(c)

Fig. 5 (a)Evolution of turbulent kinetic energy, (b) skewness and flatness factors of the velocity derivatives and (c) different main lengthscales during spectral forcing (t_{ref} = 2,7.10^{-6} s)

3.3 Near-wall turbulence

Wall affects turbulence through a number of different mechanisms. In this case, mean shear has been eliminated to consider only the interaction between turbulence and a solid stationary wall. The goal of this part is to confront results of our software to Perot and Moin's results [9]. The solid wall is inserted into isotropic turbulence decay, immediately after a large-eddy turnover time τ_k. Spectral forcing is confined inside a plane layer of fluid in order to avoid boundary influences.

Detailed instantaneous and statistical measurements of the flow have been calculated, including terms in the Reynolds stress evolution. Transport equations for the elements of the Reynolds stress tensor can be derived form the Navier-Stokes equations [9]. For the flow in question, which is homogeneous in planes parallel to the solid wall, the mean gradients in the surface-parallel directions vanish. Reynolds stress equations for $\overline{u^2}$ (tangential component of velocity) and $\overline{v^2}$ (normal component of velocity) reduce to:

$$\frac{\partial}{\partial t}\overline{u^2} = -\frac{\partial}{\partial y}\overline{u^2 v} + 2\overline{\frac{p}{\rho}\left(\frac{\partial u}{\partial x}\right)^2} - 2\upsilon\overline{\left(\frac{\partial u}{\partial x_k}\right)^2} + \upsilon\frac{\partial^2}{\partial y^2}\overline{u^2}$$

$$\frac{\partial}{\partial t}\overline{v^2} = -\frac{\partial}{\partial y}\left(\overline{v^3} + \frac{2}{\rho}\overline{pv}\right) + 2\overline{\frac{p}{\rho}\left(\frac{\partial v}{\partial y}\right)^2} - 2\upsilon\overline{\left(\frac{\partial v}{\partial x_k}\right)^2} + \upsilon\frac{\partial^2}{\partial y^2}\overline{v^2} \qquad (10)$$

We focus on the pressure-strain terms and components of the Reynolds stress tensor. Fig. 6 shows scaled Reynolds stress profiles at $t/\tau_k = 1.1$. Like Perrot & Moin, we can observe a peak near the wall which is a residual effect of the inhomogeneous initial condition at the time of wall insertion. This initial peak in tangential Reynolds stress is quickly dissipated by the viscous damping near the wall and the profiles soon collapse to a single profile when scaled appropriately. Concerning the normal Reynolds stress, the profile at this time is a good approximation to the inviscid Hunt & Graham [9] solution.

Note that, as the turbulent Reynolds number increases, the profiles become steeper at the wall but do not penetrate farther into the flow.

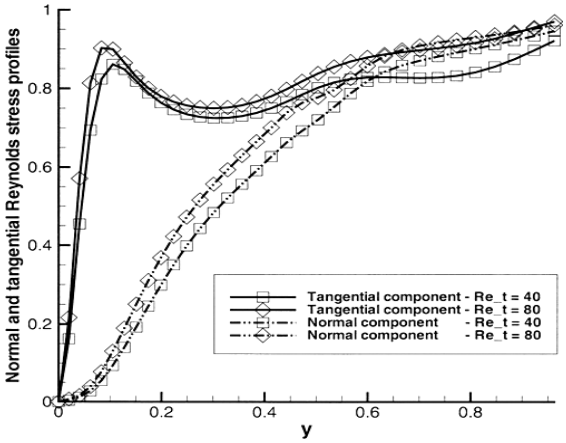

Fig. 6 Scaled Reynolds stress profiles at $t/\tau_k = 1.1$

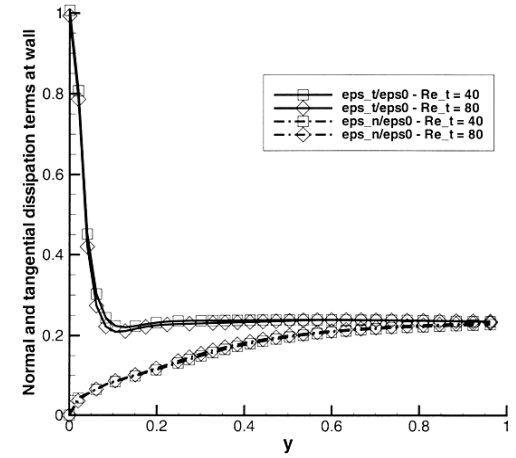

(a) Dissipation terms

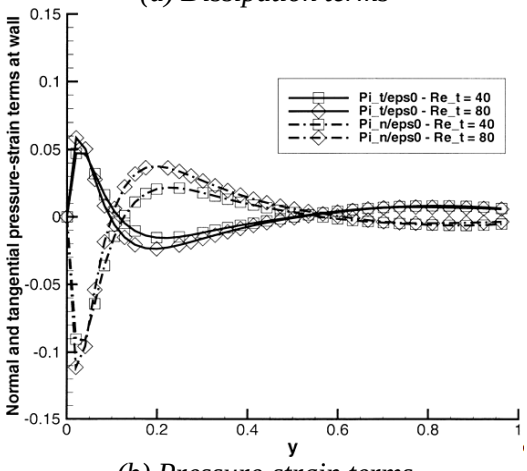

(b) Pressure-strain terms

Fig. 7 Dissipation terms (a) and pressure-strain correlations terms (b) in the transport equations for $\overline{u^2}$ and $\overline{v^2}$ Reynolds stress normalized with $\overline{\varepsilon}_{t=0}$.

Fig. 6 presents, for $\overline{u^2}$ (red) and $\overline{v^2}$ (blue), the loss due to viscous dissipation (Fig. 7.a) and pressure-strain correlations (Fig. 7.b) which represents inter-component energy redistribution near a stationary solid wall at $t/\tau_k=5$.

As might be expected for a flow with strict boundary conditions on the tangential velocity, the tangential dissipation terms ε_{trans} are large near the boundary contrary to the normal dissipation terms ε_{norm} which are relatively small (fig 7.a). The other term of importance in the balance is the pressure-strain term. Normal pressure-strain Π_{norm} dominates the near-wall balance. Its sign is negative very close to the wall (transferring energy to the tangential Reynolds stresses) but positive farther away from the wall due to the standard return-to-isotropy mechanisms (fig 7.b). The relative importance of the pressure-strain increases as the Reynolds number increases. However the extent of the pressure-strain term does not change significantly.

3.4 Ablation simulation

The ablation model considers only the sublimation reaction of C_3 at the wall. So, the preserving mass flux equation becomes:

$$-\rho D_\alpha \frac{\partial C_\alpha}{\partial y} + \rho C_\alpha v_\omega = \dot{\omega}_\alpha = J_\alpha^{sub} \qquad (11)$$

Sublimation mass flux is given by the Knudsen-Langmuir's relation:

$$J_{C_3}^{sub} = \alpha_{C_3}\left(\overline{p}_{C_3} - p_{C_3}\right)\sqrt{\frac{M_{C_3}}{2\pi RT}} \qquad (12)$$

$$J_\alpha^{sub} = 0 \quad \text{if} \quad \alpha \neq C_3$$

Where $\overline{p}_{C_3}$ and p_{C_3} are respectively the saturated vapor pressure and the partial pressure of C_3. The wall injection velocity of ablative gaseous products v_ω is determined by the mass injection rate $\dot{m}$ by:

$$\dot{m} = J_{C_3}^{sub} = \rho_\omega v_\omega \qquad (13)$$

with ρ_ω the gaseous density at wall. Considering ρ_s the heat shield material density, material recession velocity v_s is:

$$v_s = \frac{\rho_\omega v_\omega}{\rho_s} \tag{14}$$

So the preserving species equations become:

$$\begin{cases} -\rho D_{C_3} \dfrac{\partial C_{C_3}}{\partial y} + \rho C_{C_3} v_{C_3} = J_{C_3}^{sub} \\ -\rho D_\alpha \dfrac{\partial C_\alpha}{\partial y} + \rho C_\alpha v_\omega = 0 \\ J_{C_3}^{sub} = \rho_\omega v_\omega \end{cases} \tag{15}$$

Simulations of turbulent flows on ablatable surface are performed to understand how specific patterns appear and which turbulent flow parameters are responsible for it (Fig. 8)

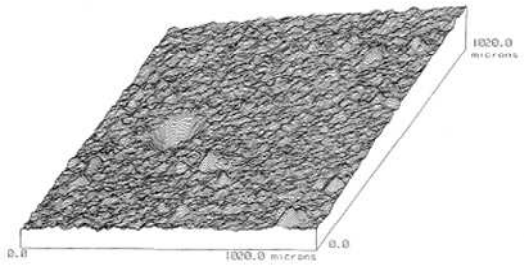

(a) Laminar flow

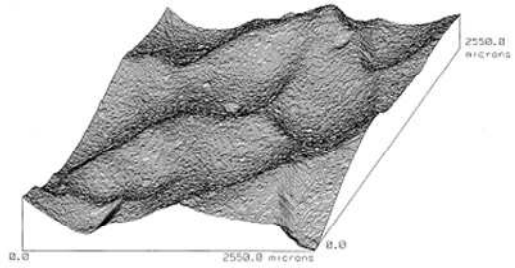

(b) Turbulent flow

Fig. 8 Polycrystalline graphite surface state after plasma jet experiments

At this point, we know that the large-eddy wavelength has no influence on recession velocity rate whereas it acts on turbulent roughness height (Fig. 9). This figure assumes that as the large-eddy wavelength increases, the magnitude of roughness height increases. Of course, it has modified surface patterns obtained (Fig. 10). The surface patterns for κ_e=6 is rougher than the one for κ_e=4.
On this figure, the wave length κ_e is an important parameter who determines the density and the magnitude of the roughness.

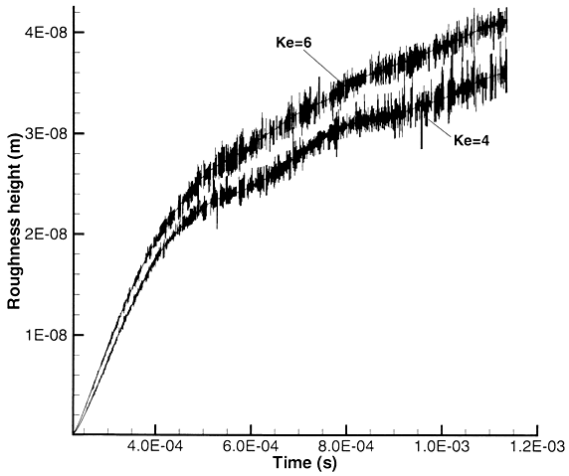

Fig. 9 Roughness height evolution for a κ_e=4 flow and a κ_e=6 flow (Re_t=90)

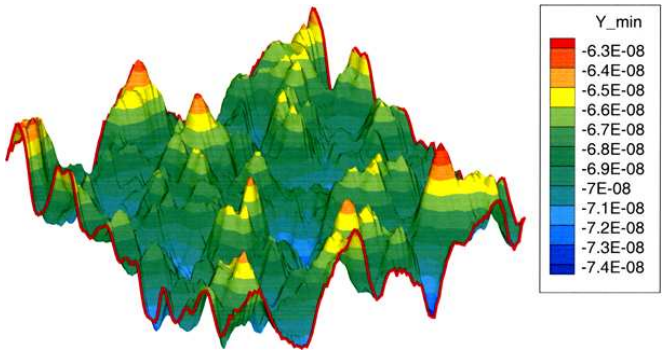

(a) κ_e=4

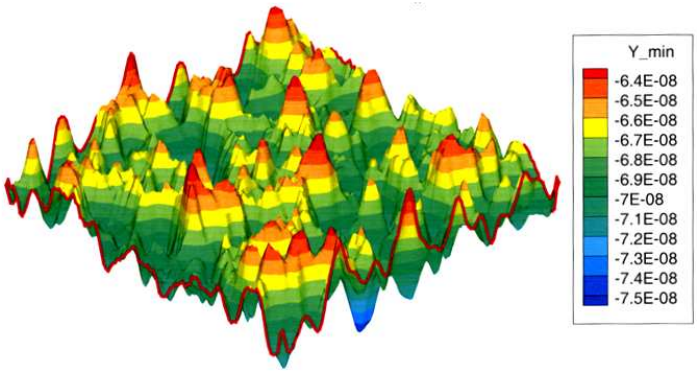

(b) κ_e=6

Fig. 10 Surface state obtained for a κ_e=4 flow (a) and a κ_e=6 (b) flow with Re_t=90

4 Conclusion and perspectives

These simulations have shown that our software is able to simulate accurate turbulent flows with several boundary conditions (periodic box and solid wall) in regard to results exposed in [7], [8] and [9]. The spectral forcing implemented is very useful in order to guarantee a steady state of turbulence without degeneration. Furthermore, we have developed a way to investigate the kinetic energy redistribution by modeling small eddies appearance. Finally we have started to identify parameters responsible for roughness appearance and roughness velocity formation rate.

Next numerical experiments will deal with ablation more exhaustively in order to identify all parameters which generate surface patterns modification. It would be interesting to take thermal transfer and pyrolysis into account by considering a solid body instead of mere boundary conditions.

References

[1] S.K. Lele, 'Compact finite difference schemes with spectral-like resolution', *Journal of Computational Physics*, 1992, vol. 103, pp 16-42.

[2] W.C. Reynolds, 'The potential and limitations of direct and large eddy simulations', in *Whither Turbulence*, 1991, vol. 357, pp 313-315

[3] T. Poinsot and S.K. Lele, 'Boundary conditions for direct simulations of compressible viscous flows', *Journal of Computational Physics*, 1992, vol. 101, pp 104-129

[4] A. Velghe, N.T.H. Nguyen-Bui, and P. Chassaing, Direct numerical simulation of reacting turbulent flow on ablatable surface, *AIAA Paper 2007-4400*, 39th AIAA Thermophysics Conference (2007).

[5] J.O. Hinze, '*Turbulence*', McGraw Hill, Oxford, first edition, 1959

[6] S.R. Rogallo, '*Numerical experiments in homogeneous turbulence*', NASA Technical Memo, n°813151 198

[7] G. Comte-Bellot and S. Corrsin, 'The use of a contraction to improve the isotropy of grid-generated turbulence', *Journal of Fluid Mech*, 1965, vol. 25, part 4, pp 657-682

[8] V. Yakhot and S.A. Orszag, 'Renormalization Group Analysis of Turbulence: 1. Basic Theory', *Journal of Scientific Computing*, 1986, 1, 3-51

[9] B. Perot and P. Moin, 'Shear-free turbulence boundary layers', *Journal of Fluid Mech*, 1995, vol. 295, pp 199-227

[10] B.E. Launder and D.B. Spalding, '*Lectures in mathematical models of turbulence*', Academic Press, London, 1972

[11] J.C. Hunt & J.M.R. Graham, 'Free-stream turbulence near plane boundaries', *Journal of Fluid Mechanics*, 1978, vol. 84, pp 161-184

Copyright Statement